Contribution from the Department of Chemistry,
University of Vermont, Burlington, Vermont 05405

Magnetic and Spectroscopic Properties of $Fe^{II}Fe^{III}_2O(CH_3CO_2)_6L_3$, L = H_2O or C_5H_5N. Direct Observation of the Thermal Barrier to Electron Transfer in a Mixed-Valence Complex

CHESTER T. DZIOBKOWSKI, JAMES T. WROBLESKI, and DAVID B. BROWN*

Received September 4, 1980

The mixed-valence iron(II, III, III) acetates $[Fe_3O(CH_3CO_2)_6L_3]$, where L = water or pyridine, have been prepared and studied by Mössbauer, infrared, and optical spectroscopy and magnetic susceptibility methods. Variable-temperature magnetic susceptibility data for the aquo complex are interpreted on the basis of an HDVV $S_2 = 2$, $S_1 = S_3 = {}^5/_2$ spin-exchange model with $J_{12} = J_{23} = -50.0$ cm^{-1} and $J_{13} = -14.5$ cm^{-1}. An intervalence-transfer band is observed at 13 800 cm^{-1} in the room-temperature electronic spectrum of the aquo complex. Mössbauer spectra of these compounds are markedly temperature dependent. At 17 K absorptions due to distinct Fe(II) and Fe(III) sites are observed while at 300 K a single absorption is observed. Spectra at intermediate temperatures are modeled by assuming intratrimer electronic relaxation between pairs of iron ions. The activation energy for relaxation derived from this model is 470 cm^{-1} for the aquo complex. This energy is equal to the barrier to intramolecular, intervalence thermal electron transfer.

Introduction

Many transition-metal ions form carboxylate complexes which have the basic iron acetate structure.[1] These complexes, of general formula $[M_3O(RCOO)_6L_3]^{n+}$, where L is a neutral, monodentate ligand, contain a triply bridging oxide ion at the center of a (generally equilateral) triangular array of metal ions. the electronic and structural properties of many of these compounds with M^{3+} ($n = 1$) have been studied. By contrast, few mixed-valence complexes with this structure have been studied in detail. Of these, $Ru_3O(CH_3CO_2)_6(PPh_3)_3$ and $Mn_3O(CH_3CO_2)_6(C_5H_5N)_3$, which formally contain $Ru^{2.67+}$ and $Mn^{2.67+}$, have been examined by single-crystal X-ray crystallography,[2,3] and both were found to contain equivalent metal ions. This structural equivalence suggests that complete electron delocalization occurs within the M_3O framework. In addition, ESCA measurements are consistent with complete electron delocalization in several similar ruthenium clusters.[4]

Although these experiments suggest that these materials are Robin and Day[5] Class III-A compounds, it has not been possible to distinguish between complete delocalization (Class III-A) and thermally activated charge transfer (Class II) in the Ru and Mn compounds. By contrast, the mixed-valence iron(II, III, III) acetates[6] $[Fe_3O(CH_3CO_2)_6L_3]$, where L = H_2O or C_5H_5N, are complexes in which the dynamics of electron transfer may be directly probed by variable-temperature ^{57}Fe Mössbauer spectroscopy. These complexes have been studied by Lupu and co-workers,[7-10] who have shown that they are Class II mixed-valence systems, because both iron(II) and iron(III) quadrupole doublets were observed in their low-temperature Mössbauer spectra. However, at room temperature only a single Mössbauer absorption was observed, suggesting that thermal electron transfer was fast on the time scale of the Mössbauer experiment (10^{-8} s). Because the experiments of Lupu were carried out over a limited temperature range and because no detailed interpretation of the resulting spectral changes was advanced, we have reexamined these compounds. The temperature dependence of the Mössbauer spectrum of this complex, which we report here, provides a unique opportunity to obtain information on the energetics and dynamics of electron transfer in a mixed-valence complex.

Experimental Section

All chemicals used were reagent grade unless specified. Pyridine was dried by refluxing with solid NaOH and purified by fractional distillation.

Preparation of Complexes. $[Fe^{II}Fe^{III}_2O(CH_3COO)_6(H_2O)_3]$. μ_3-Oxo-triaquohexakis(acetato)iron(II)diiron(III) was prepared according to a modification of the method of Chretien and Lous.[6] A solution of 60 g (0.30 mol) of $FeCl_2 \cdot 4H_2O$ in 200 mL of water was placed in a 2000-mL round-bottom flask. A suspension of 111.4 g (0.63 mol) of $Ca(CH_3CO_2)_2 \cdot H_2O$ in 178 mL of H_2O and 378 mL (6.3 mol) of concentrated acetic acid were added. The reaction mixture was continuously aerated, heated to 70 °C, and maintained at that temperature for 6 h. A reflux condenser kept evaporation to a minimum. The mixture was cooled to room temperature and the black crystalline precipitate collected by centrifugation. The product was washed twice with 50 mL of 0.083 M acetic acid, centrifuged, and dried under high vacuum. The product was stored in a sealed vial under nitrogen in a desiccator filled with nitrogen; yield 41.7 g (69.1%) Anal. Calcd for $C_{12}Fe_3H_{24}O_{16}$: C, 24.35; Fe, 28.31; H, 4.09. Found: C, 24.16; Fe, 27.90; H, 4.14.

$[Fe^{II}Fe^{III}_2O(CH_3COO)_6(C_5H_5N)_3](C_5H_5N)_{0.5}$. μ_3-Oxo-tris(pyridine)hexakis(acetato)iron(II)diiron(III) hemipyridine was prepared according to a modification of the method of Lupu and Ripan.[8] $[Fe^{II}Fe^{III}_2O(CH_3COO)_6(H_2O)_3]$ (8.5 g, 0.0144 mol) was mixed with 50 mL of pyridine which had been saturated with nitrogen gas in a nitrogen atmosphere. After 20 min of constant stirring, the black crystalline product was collected by filtration and dried under high vacuum. The product was stored in a sealed vial under nitrogen in a desiccator filled with nitrogen; yield 6.45 g (55.1%). Anal. Calcd for $C_{29.5}Fe_3H_{35.5}N_{3.5}O_{13}$: C, 43.49; Fe, 20.57; H, 4.39; N, 6.02. Found: C, 43.13; Fe, 20.55; H, 4.24; N, 6.06.

Physical Measurements. Magnetic susceptibilities, elemental analyses, Mössbauer spectra, and calculations were performed as described in the preceding work.[11] Mössbauer spectra were deconvoluted to a sum of Lorentzian absorptions plus parabolic base line with a program described by Lang and Dale.[12] Electronic spectra were obtained on a Cary 14 spectrophotometer with samples dispersed in Fluorolube grease (GR-90, Hooker Chemical Co.), between quartz plates, or dispersed in thin films of polystyrene.

Results and Discussion

Magnetic Susceptibilities. Although to date no complete crystal structure has been reported for either the mixed-valence acetate–aquo complex or its pyridine adduct, the pyridine

(1) Figgis, B. N.; Robertson, G. B. *Nature (London)* **1965**, *205*, 694. Orgel, L. E. *Ibid.* **1960**, *187*, 504.
(2) Cotton, F. A.; Norman, J. G. *Inorg. Chim. Acta* **1972**, *6*, 411.
(3) Baikie, A. R. E.; Hursthouse, M. B.; New, D. B.; Thornton, P. *J. Chem. Soc., Chem. Commun.* **1978**, 62.
(4) Wilson, S. T.; Bondurant, R. F.; Meyer, T. J.; Salmon, D. J. *J. Am. Chem. Soc.* **1975**, *97*, 2285. Baumann, J. A.; Salmon, D. J.; Wilson, S. T.; Meyer, T. J.; Hatfield, W. E. *Inorg. Chem.* **1978**, *17*, 3342.
(5) Robin, M. B.; Day, P. *Adv. Inorg. Chem. Radiochem.* **1967**, *10*, 247.
(6) Chretien, A.; Lous, E. *Bull. Soc. Chim. Fr.* **1944**, *11*, 446.
(7) Lupu, D. *Rev. Roum. Chim.* **1970**, *15*, 417.
(8) Lupu, D.; Ripan, R. *Rev. Roum. Chim.* **1971**, *16*, 43.
(9) Lupu, D.; Barb, D.; Filoti, G.; Morariu, M.; Tarina, D. *J. Inorg. Nucl. Chem.* **1972**, *34*, 2803.
(10) Grecu, R.; Lupu, D. *Rev. Roum. Chim.* **1971**, *16*, 1811.
(11) Dziobkowski, C. T.; Wrobleski, J. T.; Brown, D. B. *Inorg. Chem.*, preceding paper in this issue.
(12) Lang, G.; Dale, B. W. *Nucl. Instrum. Methods* **1974**, *116*, 567.

0020-1669/81/1320-0679$01.00/0

adduct has been reported to be isostructural with the manganese analogue.[3] Because the manganese complex contains an equilateral triangle of metal ions, it is probable that this geometry holds for the aquo, as well as the pyridine, iron complex. However, as shown by the Mössbauer spectra (vide infra), on some time scale the iron sites are electronically distinguishable. Consequently the system may be treated in the Heisenberg–Dirac–Van Vleck (HDVV) formalism as an $S_2 = 2$, $S_1 = S_3 = {}^5/_2$ trimer. As described by Kambe,[13] the appropriate spin Hamiltonian is

$$\mathcal{H} = -2J(S_1 \cdot S_2 + S_2 \cdot S_3) - J'(S_1 \cdot S_3) \qquad (1)$$

where J = Fe(II)–Fe(III) exchange parameter, J' = Fe(III)–Fe(III) exchange parameter, and S_i = spin on the individual ion (S_1, S_3, Fe(III); S_2, Fe(II)). The expression for the energy (eq 2) of each spin state can be derived in the

$$E(S^*,S') = \frac{2ZJ}{n-1}[S'(S'+1) - S^*(S^*+1)] - \frac{ZJ'}{n-1}[S^*(S^*+1)] \qquad (2)$$

normal manner,[14] where $E(S^*,S')$ = energy of a spin state, Z = number of nearest neighbors (=2), n = number of interacting paramagnetic ions (=3), $S^* = S_1 + S_3$, $S_1 + S_3 - 1$, ..., 0, and $S' = S^* + S_2$, $S^* + S_2 - 1$, ..., 0. When the energies are substituted into the appropriate molar susceptibility partition function,[14] the result is the working expression for the theoretical molar susceptibility (eq 3, where $X = J/kT$ and $Y = J'/kT$). We have included this equation because it disagrees, in several terms, with that which has previously been reported by Lupu.[7]

$$\begin{aligned}\chi_M = \{N\beta^2g^2[&840\exp(-26X-30Y) + 546\exp(-12X-30Y) + 330\exp(-30Y) + 180\exp(10X-30Y) + \\ &84\exp(18X-30Y) + 546\exp(-22X-20Y) + 330\exp(-10X-20Y) + \\ &180\exp(-20Y) + 84\exp(8X-20Y) + 30\exp(14X-20Y) + 330\exp(-18X-12Y) + \\ &180\exp(-8X-12Y) + 84\exp(-12Y) + 30\exp(6X-12Y) + 6\exp(10X-12Y) + 180\exp(-14X-6Y) + \\ &84\exp(-6X-6Y) + 30\exp(-6Y) + 6\exp(4X-6Y) + 84\exp(-10X-2Y) + \\ &30\exp(-4X-2Y) + 6\exp(-2Y) + 30\exp(-6X)]\}/ \\ \{3kT[&15\exp(-26X-30Y) + 13\exp(-12X-30Y) + 11\exp(-30Y) + 9\exp(10X-30Y) + 7\exp(18X-30Y) + \\ &13\exp(-22X-20Y) + 11\exp(-10X-20Y) + 9\exp(-20Y) + 7\exp(8X-20Y) + 5\exp(14X-20Y) + \\ &11\exp(-18X-12Y) + 9\exp(-8X-12Y) + 7\exp(-12Y) + 5\exp(6X-12Y) + 3\exp(10X-12Y) + \\ &9\exp(-14X-6Y) + 7\exp(-6X-6Y) + 5\exp(-6Y) + 3\exp(4X-6Y) + 1\exp(6X-6Y) + \\ &7\exp(-10X-2Y) + 5\exp(-4X-2Y) + 3\exp(-2Y) + 5\exp(-6X)]\} \qquad (3)\end{aligned}$$

Lupu[7] measured the susceptibility of the aquo complex over the range of 94–296 K. Exchange parameters were obtained by finding the best fit of the experimental susceptibility to the (incorrect) theoretical expression at a *single* temperature. This procedure, repeated at two other temperatures, led to exchange parameters which were themselves temperature dependent; that is, the values of J ranged from +2.8 cm^{-1} at 101 K to −10 cm^{-1} at 288 K. We have measured the susceptibility over the range 17–294 K. The data are given in Table I[15] and shown graphically in Figure 1. Over the coincident temperature range, the data are in excellent agreement with those reported by Lupu. The data have been fit to eq 3 by employing the Simplex minimization algorithm.[16,17] The best fit, assuming $g = 2.00$, is shown as the solid curve in Figure 1. The calculated values of the exchange parameters are $J = -50.0$ and $J' = -14.5$ cm^{-1} ($J/J' = 3.47$). Although a direct comparison of exchange parameters in similar iron(III) compounds is difficult to make, these values have an average near that of, for example, $[Fe_3O(CH_3CO_2)_6(H_2O)_3]ClO_4$.[11] The success of eq 3 at describing the susceptibility of the aquo complex suggests that it, like the pyridine complex, does adopt the basic iron acetate structure.

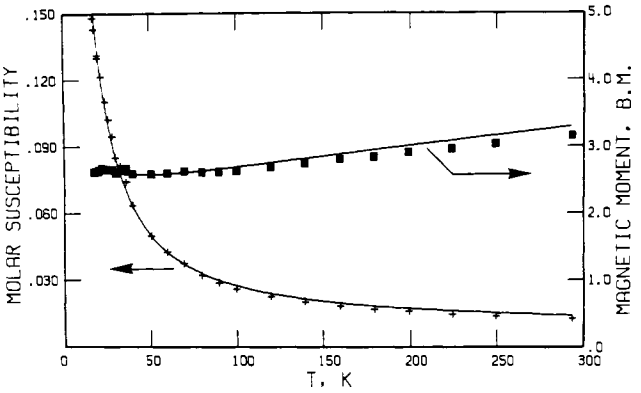

Figure 1. Molar magnetic susceptibility and effective magnetic moment vs. temperature for $[Fe^{II}Fe^{III}_2O(CH_3COO)_6(H_2O)_3]$. The solid line gives the theoretical fit to the HDVV model with $S_1 = S_3 = {}^5/_2$ and $S_2 = 2$ with $J = -50.0$ cm^{-1}, $J' = -14.5$ cm^{-1}, and $g = 2.00$.

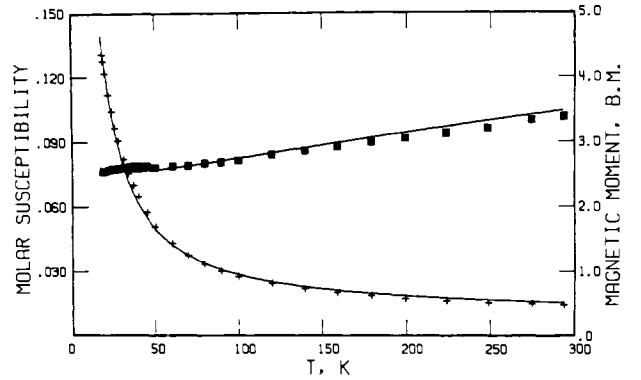

Figure 2. Molar magnetic susceptibility and effective magnetic moment vs. temperature for $[Fe^{II}Fe^{III}_2O(CH_3COO)_6(C_5H_5N)_3]\cdot(C_5H_5N)_{0.5}$. The solid line gives the theoretical fit to the HDVV model with $S_1 = S_3 = {}^5/_2$ and $S_2 = 2$ with $J = -37.2$ cm^{-1}, $J' = -14.5$ cm^{-1}, and $g = 2.00$.

The relatively much stronger Fe(II)–Fe(III) exchange integral reflects in part the greater number of pathways available for this exchange. Its larger value is, moreover, consistent with the Mössbauer results (vide infra) which demonstrate that electronic relaxation between Fe(II) and Fe(III) sites is much more facile than that between Fe(III) and Fe(III) sites.

The pyridine complex has a temperature-dependent susceptibility which is similar to the aquo complex. The data and

(13) Kambe, K. *J. Phys. Soc. Jpn.* **1950**, *5*, 48.
(14) Mabbs, F. E.; Machin, D. J. "Magnetism and Transition Metal Complexes"; Chapman and Hall: London, 1973; pp 190–196.
(15) Supplementary material.
(16) Deming, S. N.; Morgan, S. L. *Anal. Chem.* **1973**, *45*, 278A.
(17) Dean, W. K.; Heald, K. J.; Deming, S. N. *Science (Washington, D.C.)* **1975**, *189*, 805.

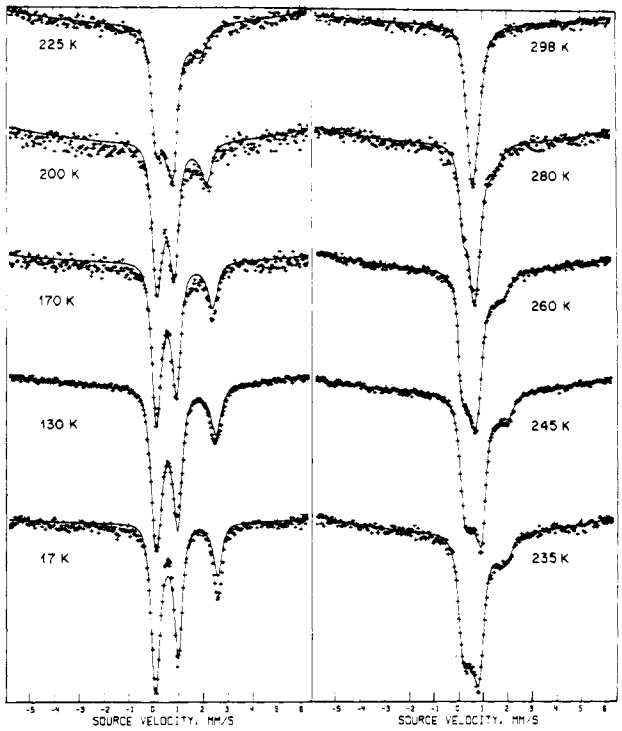

Figure 3. Variable-temperature Mössbauer spectra of the aquo complex (9 mg of Fe/cm^2, sample dispersed in Vaseline). The solid lines represent theoretical fits obtained by using the relaxation model described in the text.

best fit to eq 3 are shown in Figure 2 and detailed in Table II.[15] The exchange parameters $J = -37.2$ and $J' = -11.2$ cm^{-1} are somewhat larger than in the aquo complex, whereas the ratio $J/J' = 3.32$ is similar to that of the aquo complex.

Mössbauer Spectra. Aquo Complex. Representative variable-temperature (17–298 K) Mössbauer spectra of the mixed-valence aquo complex are illustrated in Figure 3. At 17 K the spectrum consists of three clearly resolved absorptions. As the temperature is increased, the resonant absorptions coalesce, and the apparent intensity of the high velocity line decreases. The final spectrum at 298 K has the appearance of a single broadened absorption centered at approximately 0.75 mm/s. These changes are reversible provided the sample is not heated above room temperature. At $T > 298$ K we do not observe further narrowing of the Mössbauer absorption but rather a gradual, irreversible oxidation and/or dehydration of the sample occurs, and the spectrum *broadens* as a result of the decomposition. Indeed, prolonged heating of the sample at 373 K under vacuum results in the formation of a spectrum composed of a single quadrupole doublet with $\delta = 0.6$ mm/s and $\Delta = 0.75$ mm/s. After this heat treatment the two-line spectrum persists to 17 K.

Although only three absorptions are resolved in the spectra below 200 K, it is obvious from inspection of the relative line intensities that two absorptions are *nearly* coincident at approximately 0.1 mm/s. The 17 K spectrum was fit to four absorptions with the constraint that one of the absorptions at 0.1 mm/s be equal to the high-energy absorption at ca. 2.6 mm/s and that the remaining two absorptions also be equal to one another. The two less intense absorptions were found at 0.190 and 2.589 mm/s whereas the remaining lines with larger intensity were located at 0.028 and 0.984 mm/s. Furthermore, the ratio of the areas of the 0.984 to the 2.589 mm/s absorption was 1.77. On the basis of calculated quadrupole splittings and isomer shifts the absorptions at 0.190 and 2.589 mm/s were assigned to Fe(II) transitions ($\delta = 1.39$ and $\Delta = 2.40$ mm/s) and those at 0.028 and 0.984 mm/s to

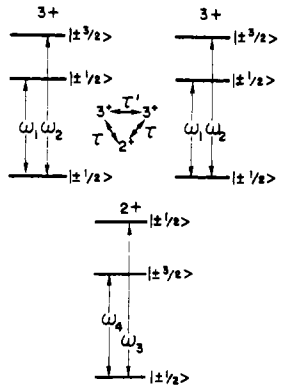

Figure 4. Illustration of the relaxation model employed to calculate Mössbauer spectra for the mixed-valence acetate trimers.

Fe(III) transitions ($\delta = 0.51$ and $\Delta = 0.98$ mm/s). Although this four-line fit is statistically acceptable ($R = 2.3$),[18] the area ratio of 1.77 is significantly less than the anticipated value of 2.0. This discrepancy is larger at higher temperatures. Thus, the Fe(III):Fe(II) area ratio increases to 2.60 at 225 K and ca. 4.0 at 280 K. We do not believe that this variable-area ratio results entirely from a difference in the temperature dependence of the recoilless fraction ratio of Fe(III) to Fe(II) sites in this material. Rather, we propose that intramolecular Fe(II) → Fe(III) thermal electron transfer is responsible for the observed temperature-dependent Mössbauer spectra (vide infra).

In order to theoretically model the Mössbauer spectra shown in Figure 3, we adopted the relaxation model which is illustrated in Figure 4. The spectral transitions, ω_i, are given in units of mm/s in Figure 4. The mathematical formalism which was applied to this relaxation model is based on the quantum mechanical density matrix equations of motion dG_i/dt given by Wickman.[19] Details of the mathematics will not be given here. However, it is important to briefly sketch the important computational features of the model. Theoretical Mössbauer spectra were calculated from the known solution to the equations of motion, which is, in this instance, expressed by eq 4. In eq 4 the subscript i refers to an individual Mössbauer

$$I_2(\omega) = \sum_i^{i} [(1 + \tau_i\Gamma_i)P_i + Q_iR_i]/(P_i^2 + R_i^2) \qquad (4)$$

transition, $P_i = \tau_i[\Gamma_i^2 - (\Delta_i' - \omega)^2 + \delta_i'^2] + \Gamma_i$, $R_i = (\Delta_2' - \omega)(1 + 2\tau_i\Gamma_i)$, $Q_i = \tau_i(\Delta_i' - \omega)$, and Γ_i is the line width for transition i. In our model, relaxation processes occur between Fe^{2+} and Fe^{3+} nuclear energy levels (3+ ↔ 2+) and also between pairs of Fe^{3+} nuclear energy levels (3+ ↔ 3+). It is therefore necessary to compute the Mössbauer spectrum for *six* transition frequencies which enter eq 4 through the Δ_i' and δ_i' terms given in eq 5. The model was constructed with equal

$$\begin{aligned}
\Delta_1' &= \tfrac{1}{2}(\omega_1 + \omega_3) & \delta_1' &= \tfrac{1}{2}(\omega_1 - \omega_3) \\
\Delta_2' &= \tfrac{1}{2}(\omega_2 + \omega_4) & \delta_2' &= \tfrac{1}{2}(\omega_2 - \omega_4) \\
\Delta_3' &= \Delta_2' & \delta_3' &= \tfrac{1}{2}(\omega_4 - \omega_2) \\
\Delta_4' &= \Delta_1' & \delta_4' &= \tfrac{1}{2}(\omega_3 - \omega_1) \\
\Delta_5' &= \omega_1 & \delta_5' &= \delta_6' = 0 \\
\Delta_6' &= \omega_2 & & \qquad (5)
\end{aligned}$$

probability for all transitions. Furthermore the 3+ ↔ 3+ relaxation time was assumed to be much longer than the nu-

(18) R is defined as the ratio of the normalized sum of the squares of the residuals to the number of degrees of freedom in the fit.
(19) Wickman, H. H. "Mössbauer Effect Methodology"; I. J. Gruverman, Ed.; Plenum Press: New York, 1966; p 39.

Table III. Mössbauer Spectral Data for the Aquo Complex

T, K	δ(Fe(II)), mm/s[a]	δ(Fe(III)), mm/s[a]	Δ(Fe(II)), mm/s	Δ(Fe(III)), mm/s	τ, ns
17.0	1.35	0.52	2.52	0.99	>2444
130.0	1.34	0.50	2.38	0.95	196
170.0	1.28	0.51	2.28	0.89	116
200.0	1.24	0.49	2.21	0.83	95.3
210.0	1.20	0.49	2.00	0.79	62.7
225.0	1.19	0.52	1.70	0.74	21.5
235.0	1.14	0.52	1.64	0.72	22.0
245.0	1.15	0.54	1.66	0.72	20.4
260.0	1.14	0.54	1.56	0.68	18.0
280.0	1.06	0.55	1.10	0.58	11.6
298.0	0.99	0.56	0.77	0.24	2.5

[a] Relative to α-Fe.

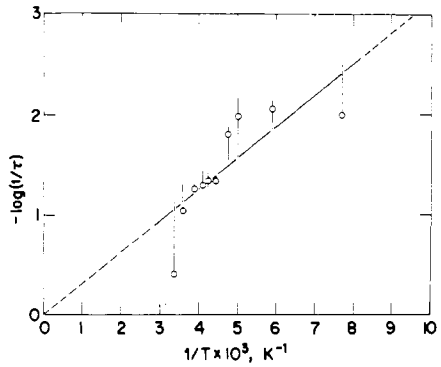

Figure 5. Plot of $-\log(1/\tau)$ vs. $1/T$ for the aquo complex. The "uncertainty bars" are described in the text. The straight line is a least-squares fit to the open circles and results in an activation energy of 470 cm^{-1}.

clear excited-state lifetime (99.7 ns) and was arbitrarily set at 200 ns. Arbitrarily longer 3+ ↔ 3+ relaxation times had no obvious effect on the calculated spectra. The line width for 2+ ↔ 3+ transitions was assumed to be equal to the natural line width (0.1946 mm/s) whereas the 3+ ↔ 3+ line width was empirically determined to be 0.30 ± 0.05 mm/s and therefore was set at 0.30 mm/s for all calculations.

In fitting the experimental spctra to this model the Fe^{2+} and Fe^{3+} isomer shifts and quadrupole splittings were parameterized as well as the 2+ ↔ 3+ relaxation time. Computer minimization of eq 4 resulted in the theoretical spectra illustrated as smooth curves in Figure 3. "Best fit" values of δ(Fe(II)), δ(Fe(III)), Δ(Fe(II)), Δ(Fe(III)), and τ(2+ ↔ 3+) are given in Table III. Values of τ(2+ ↔ 3+) calculated in this manner are presented as an Arrhenius activation energy plot in Figure 5. In Figure 5 the open circles refer to relaxation times which were obtained by direct minimization in the manner previously outlined. The range of relaxation time values at each temperature, represented by lines parallel to the $-\log(1/\tau)$ axis, is intended to illustrate the relative uncertainty in τ according to this model. These "uncertainty bars" were obtained by holding δ(Fe(II)), δ(Fe(III)), Δ(Fe(II)), and Δ(Fe(III)) constant and changing τ(2+ ↔ 3+) until the sum of squares was doubled. In some instances, particularly at the low- and high-temperature limits, the calculated spectra are quite insensitive to variations in τ(2+ ↔ 3+). However at intermediate relaxation times the spectra are quite sensitive to rather small (~2 ns) changes in τ. For extraction of an energy barrier from these data, the open circle points were least-squares fit to a straight line. The result of this fit is illustrated as the line in Figure 5. The slope of this line is 303 K. By employing the relation $E = 2.303 k_B \cdot \text{slope}$, where k_B is Boltzmann's constant, we obtain an activation energy of 470 cm^{-1}. Because of the definition of τ(2+ ↔ 3+) in this model, E may be interpreted as the *thermal barrier to electron transfer* in this mixed-valence trimer. The magnitude of this barrier has a rather large uncertainty, as it is obvious that the fit of Figure 5 is not unique. Furthermore, non-Arrhenius behavior may be more appropriate in this case.[20] However, because the data at the high- and low-temperature extremes are so insensitive to the choice of τ, we do not believe that the use of more complicated, nonlinear, fits to the data are justified.

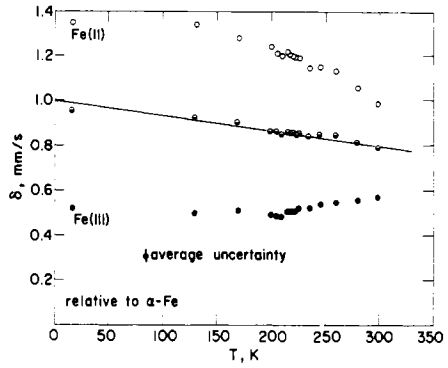

Figure 6. Plot of the temperature dependence of derived isomer shifts for the Fe(II) (open circles), Fe(III) (filled circles), and average oxidation state (half-filled circles) sites in the aquo complex. The solid line represents the second-order Doppler shift correction to the isomer shift of the average oxidation state.

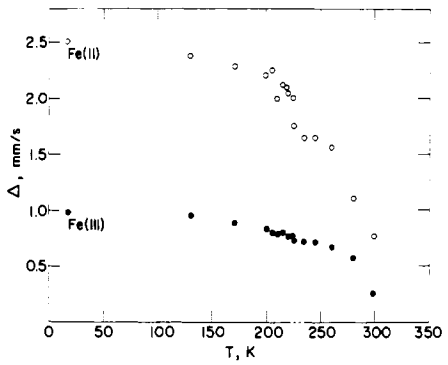

Figure 7. Plot of the temperature variation of the derived quadrupole splittings of the Fe(II) (open circles) and Fe(III) (filled circles) sites in the aquo complex.

Figure 6 illustrates the temperature dependence of the isomer shift of the Fe(II) and Fe(III) sites, shown as open and filled circles, respectively. Because these isomer shifts are not corrected for second-order Doppler shift effects, it appears that the Fe(II) isomer shift is decreasing at a much greater rate than the Fe(III) isomer shift is increasing. In the absence of second-order Doppler effects, the isomer shifts are seen to converge at approximately 350 K. The second-order Doppler effect may be visualized by plotting the *average* of the Fe(II) and Fe(III) isomer shifts. These average δ values are shown as half-filled circles in Figure 6. The straight line drawn through these points represents the high-temperature limiting form of the second-order Doppler shift (slope = 6.3 × 10^{-4} mm/s K^{-1}).

The temperature variation of the quadrupole splitting for both Fe(II) and Fe(III) sites is illustrated in Figure 7. These quadrupole splittings are apparently converging to approximately zero between 320 and 350 K. This averaging of quadrupole splittings to zero is taken account of in the model by assuming that the $|\pm^1/_2\rangle$ excited nuclear energy level lies above the $|\pm^3/_2\rangle$ level (see Figure 4); that is to say, Δ is negative for the Fe(II) sites in this complex. An average quadrupole splitting of zero in this case is only possible if Δ(Fe(II)) and Δ(Fe(III)) are of opposite sign.

(20) LaPlante, J.-P.; Siebrand, W. *Chem. Phys. Lett.* **1978**, *59*, 433.

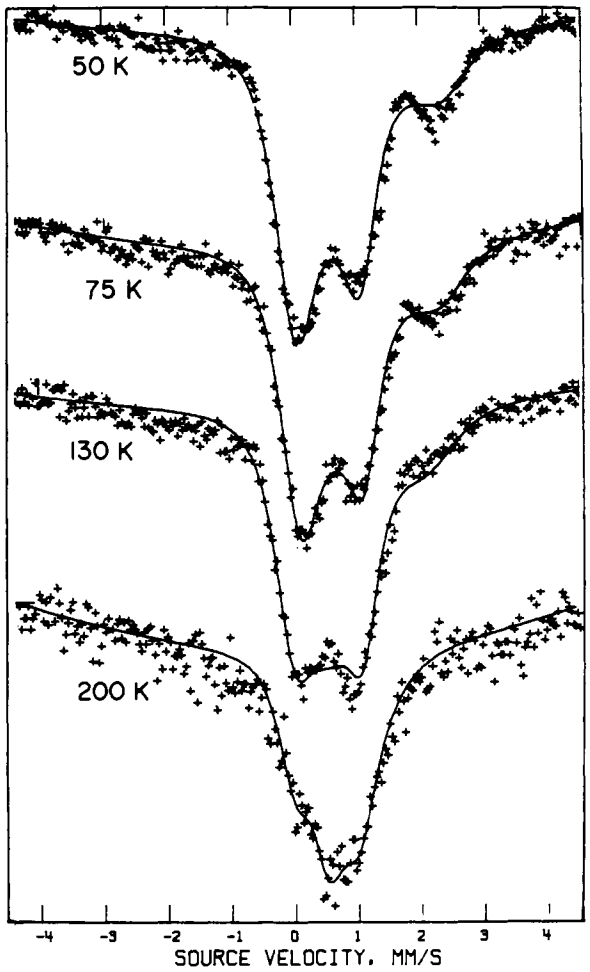

Figure 8. Representative variable-temperature Mössbauer spectra of the pyridine mixed-valence trimer. The solid lines represent theoretical fits obtained by using the relaxation model described in the text.

Table IV. Mössbauer Spectral Data for the Pyridine Complex

T, K	δ(Fe(II)), mm/s[a]	δ(Fe(III)), mm/s[a]	Δ(Fe(II)), mm/s	Δ(Fe(III)), mm/s	τ, ns
16.8	1.18	0.56	2.85	1.08	>200
50.0	1.14	0.55	2.80	1.06	11.5
75.0	1.16	0.55	2.61	1.06	11.7
130.0	1.17	0.52	2.39	1.12	9.7
195.0	1.05	0.51	1.80	1.06	8.0
200.0	0.91	0.50	1.77	1.03	5.4

[a] Relative to α-Fe.

Pyridine Complex. The gross features of the variable-temperature Mössbauer spectra of the pyridine complex are similar to those of the aquo complex. A number of details of the spectra are diferent, however. The representative spectra illustrated in Figure 8 point out some of the differences. First, the pyridine complex possesses a much smaller recoilless fraction than the aquo complex. This smaller f value is reflected in the statistically poorer pyridine spectra. Only very poorly resolved spectra were obtained above 200 K. Because of the poor quality of the high-temperature spectra, we were unable to extract meaningful δ, Δ, and τ parameters through application of our relaxation model. At lower temperatures, however, we were able to obtain useful spectral parameters for the relaxation process. These values are listed in Table IV. A plot of $-\log(1/\tau)$ vs. $1/T$ gives an activation energy of 150 cm^{-1} for the thermal electron-transfer barrier in the pyridine complex. This value is however subject to a large uncertainty because of the relative insensitivity of the spectra to rather large changes in $\tau(2+ \leftrightarrow 3+)$. A smaller value of E for the pyridine relative to the aquo complex is, nonetheless, indicated by the fact that the Mössbauer spectrum of the pyridine complex shows rapid electron transfer at approximately 200 K whereas this rapid electron transfer is only observed at ca. 300 K in the aquo complex.

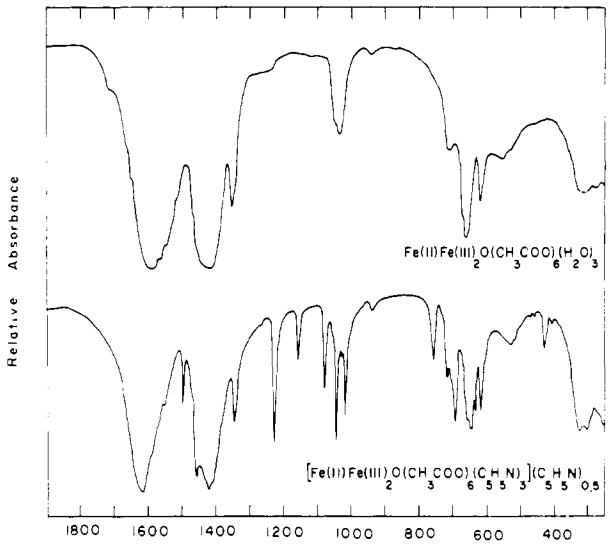

Figure 9. Infrared spectra of the mixed-valence acetate complexes.

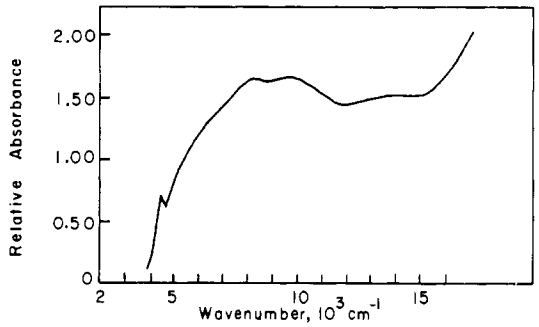

Figure 10. Room-temperature electronic spectrum of $Fe_3O(CH_3CO_2)_6(H_2O)_3$.

Infrared Spectra. Infrared spectra for the mixed-valence acetate complexes are shown in Figure 9, and band assignments are listed in Tables V and VI.[15] Vibrations were assigned with use of the conventions of Nakamoto[21] and are, for the most part, consistent with the assignments of Grecu and Lupu.[10] Of particular importance is an absorption near 530 cm^{-1} which has been assigned[10] to the asymmetric stretch of the Fe_3O core [$\nu_s(Fe_3O)$]. This same absorption is present in the singly valent Fe(III) complexes,[22] although Griffith[23] has assigned this mode to an absorption at 588 cm^{-1}. For the local D_{3h} symmetry of the M_3O core, the symmetric stretching mode [$\nu_s(Fe_3O)$] is Raman, but not infrared, active. Although no Raman data have been reported for any of the mixed-valence complexes, Griffith[23] has assigned a Raman band at 181 cm^{-1} in the Fe(III) complex to this absorption.

Electronic Spectra. Figure 10 shows the room-temperature electronic spectrum of $Fe_3O(CH_3CO_2)_6(H_2O)_3$. Broad absorptions at 8200 and 9700 cm^{-1} are typical of the $Fe^{II}O_6$ chromophore, and the singly valent Fe(III) analogue exhibits absorptions in this region as well.[22] We assign the absorption at 13 800 cm^{-1}, which is not present in the singly valent complex, to an intervalence-transfer band. Intervalence-transfer

(21) Nakamoto, K. "Infrared Spectra of Inorganic and Coordination Compounds"; Wiley: New York, 1970.
(22) Long, G. J.; Robinson, W. T.; Tappmeyer, W. R.; Bridges, D. L. *J. Chem. Soc., Dalton Trans.* **1973**, 573.
(23) Griffith, W. P. *J. Chem. Soc. A* **1969**, 2270.

absorptions have been observed in this region in other single-atom-bridged Fe(II, III) complexes,[24] but the lack of resolution of this band precludes detailed analysis.

Conclusions. Data obtained from a variety of physical methods demonstrate that the mixed-valence iron(II, III, III) acetates undergo dynamic intratrimer electron-transfer. With ^{57}Fe Mössbauer spectroscopy, rate constants for the intervalence transfer have been determined. Although the precision is not high, the barriers to thermal electron transfer have been extracted with use of an Arrhenius activation model. Recent theoretical work[25] has shown that many of the spectral properties of mixed-valence compounds are explicable in terms of a vibronic coupling model. For a symmetrical mixed-valence complex (such as is the case here) thermal intervalence-transfer should be a phonon-assisted process in which the ions are coupled by the asymmetric stretching vibrational mode of the interacting ions. It may prove possible to interpret the temperature dependence of the Mössbauer spectra with use of the vibronic coupling model for the electron-transfer process or with other models which consider tunnelling transitions explicitly. Such interpretations, however, must await more detailed theoretical and experimental examination.

These compounds have provided a unique opportunity to determine directly the energetics of thermal electron transfer. This thermal barrier has been determined in only one other molecular system.[26] Gagné and co-workers have used EPR measurements to estimate the electron-transfer rate, and thus the activation energy, in a binuclear copper(I, II) complex. Other compounds, such as the Creutz and Taube (C-T) complex $[(NH_3)_5Ru\text{-}pyr\text{-}Ru(NH_3)]^{5+}$ (pyr = pyrazine), exhibit apparent[27] thermally activated electron transfer, but experimental probes to measure the barrier directly are not available. Thus, although electron transfer is known to be fast at room temperature, on the time scale of ^{99}Ru Mössbauer spectroscopy (ca. 10^{-9} s) valences are trapped at 4 K.[28] The same types of information which we have obtained for the mixed-valence iron acetate are, in principle, obtainable from temperature-dependent ^{99}Ru Mössbauer spectroscopy. Unfortunately, low recoil-free fractions preclude the observation of ^{99}Ru Mössbauer spectra at temperatures where thermally activated electron transfer is facile.

The thermal barrier to electron transfer has been measured by using Mössbauer spectroscopy in other cases. With ^{151}Eu Mössbauer spectroscopy, Eu_3S_4 has been shown to undergo intervalence electron hopping with an activation energy of 0.24 eV.[29] Electron hopping in this system, a continuous lattice semiconductor, can be correlated with the activation energy of 0.22 eV determined from electrical conductivity measurements. The semiconductor Sn_2S_3 has also been studied by variable-pressure ^{119}Sn Mössbauer spectroscopy.[30] The results of this study are, however, more consistent with a "valence polarization" rather than true electron transfer in Sn_2S_3. Thus, $Fe_3O(CH_3CO_2)_6(H_2O)_3$ and its pyridine analogue provide a unique probe to the dynamics of electron transfer in molecular mixed-valence compounds and may consequently serve as important systems on which to focus efforts on fundamental understanding of the mixed-valence phenomenon.

Acknowledgment. This work was supported in part by the Office of Naval Research. We thank Dr. E. E. Weltin for helpful discussions.

Registry No. $Fe^{II}Fe^{III}_2O(CH_3COO)_6(H_2O)_3$, 36354-69-5; $Fe^{II}Fe^{III}_2O(CH_3COO)_6(C_5H_5N)_3$, 35268-77-0.

Supplementary Material Available: Experimental and calculated magnetic susceptibilities (Tables I and II) and infrared spectral data and assignments (Tables V and VI) (6 pages). Ordering information is given on any current masthead page.

(24) Walton, E. G.; Corvan, P. J.; Brown, D. B.; Day, P. *Inorg. Chem.* **1976**, *15*, 1737.
(25) Piepho, S. B.; Krausz, E. R.; Schatz, P. N. *J. Am. Chem. Soc.* **1978**, *100*, 2996. Wong, K. Y.; Schatz, P. N.; Piepho, S. B. *Ibid.* **1979**, *101*, 2793.
(26) Gagné, R. R.; Koval, C. A.; Smith, T. J.; Cimolino, M. C. *J. Am. Chem. Soc.* **1979**, *101*, 4571.
(27) There is some controversy regarding this material, particularly with respect to a trapped vs. delocalized ground-state description. Arguments favoring a trapped (Class II) ground state are summarized in: Bunker, B. C.; Drago, R. S.; Hendrickson, D. N.; Richman, R. M.; Kessell, S. L. *J. Am. Chem. Soc.* **1978**, *100* 3805. Arguments favoring a delocalized (Class III) ground state are detailed in: Hush, N. S. "Mixed-Valence Compounds"; Brown, D. B., Ed.; Reidel: Dordrecht, The Netherlands, 1980; p 151.
(28) Creutz, C.; Good, M. L.; Chandra, S. *Inorg. Nucl. Chem. Lett.* **1973**, *9*, 171.
(29) Berkooz, O.; Malamud, M.; Shtrikman, S. *Solid State Commun.* **1968**, *6*, 185.
(30) Amthauer, G.; Fenner, J.; Hafner, S.; Holzapfel, W. B.; Keller, R. *J. Chem. Phys.* **1979**, *70*, 4837.

Contribution from the Department of Chemistry, University of Vermont, Burlington, Vermont 05405

Reanalysis of the Thermal, Magnetic, and Spectral Properties of $[Cr_3O(CH_3COO)_6(H_2O)_3]Cl\cdot 6H_2O$ on the Basis of an Intercluster Spin-Exchange Model

JAMES T. WROBLESKI, CHESTER T. DZIOBKOWSKI, and DAVID B. BROWN*

Received September 4, 1980

Inclusion in the Hamiltonian of a perturbing term which describes spin exchange between equilateral triangle clusters in $[Cr_3O(CH_3COO)_6(H_2O)_3]Cl\cdot 6H_2O$ splits the ground state into two nondegenerate Kramers doublets. This splitting introduces a Schottky anomaly in the theoretical heat capacity curve. Two inequivalent pairs of trimer sites with different intercluster-exchange parameters are required to obtain agreement between experimental and theoretical heat capacities, low-temperature magnetic susceptibility data, and optical spectral data.

Previous theoretical models[1-6] proposed to account for the low-temperature thermal and magnetic susceptibility behavior of $[Cr_3O(CH_3COO)_6(H_2O)_3]Cl\cdot 6H_2O$ have been based on structural assumptions which are not substantiated by available data. These assumptions have been invoked because the

(1) J. Wucher and H. M. Gijsman, *Physica (Amsterdam)*, **20**, 361 (1954).
(2) J. Wucher and J. D. Wasscher, *Physica (Amsterdam)*, **20**, 721 (1954).
(3) J. T. Schriempf and S. A. Friedberg, *J. Chem. Phys.*, **40**, 296, (1964).
(4) N. Uryû and S. A. Friedberg, *Phys. Rev. A*, **140**, 1803 (1965).
(5) M. Sorai, M. Tachiki, H. Suga, and S. Seki, *J. Phys. Soc. Jpn.*, **30**, 750 (1971).
(6) M. Mishima and N. Uryû, *Phys. Lett. A*, **67**, 64 (1978).

0020-1669/81/1320-0684$01.00/0